



Improved formation density measurement using controllable D-D neutron source and its lithological correction for porosity prediction

Li Zhang^{1,4} · Hua-Wei Yu² · Yang Li³ · Wen-Bao Jia⁴ · Xiao Han¹ ·
Xue-Sen Geng¹

Received: 15 October 2021 / Revised: 2 December 2021 / Accepted: 3 December 2021 / Published online: 15 January 2022
© The Author(s), under exclusive licence to China Science Publishing & Media Ltd. (Science Press), Shanghai Institute of Applied Physics, the Chinese Academy of Sciences, Chinese Nuclear Society 2022

Abstract Controllable D-D neutron sources have a long service life, low cost, and non-radioactivity. There are favorable prospects for its application in geophysical well logging, since traditional chemical radioactive sources used for well logging pose potential threats to the safety of the human body and environment. This paper presents an improved method to measure formation density that employs a D-D neutron source. In addition, the lithological effect on the measured density was removed to better estimate the formation porosity. First, we investigated the spatial distribution of capture gamma rays through Monte Carlo simulations as well as the relationship between the ratio of capture gamma ray counts and formation density to establish theoretical support for the design of density logging tools and their corresponding data processing methods. Second, we obtained the far to near detector counts of

captured gamma rays for an optimized tool structure and then established its correlation with the density and porosity of three typical formations with pure quartz, calcite, and dolomite minerals. Third, we determined the values for correcting the densities of sandstone and dolomite with the same porosity using limestone data as the reference and established the equations for calculating the correction values, which lays a solid foundation for accurately calculating formation porosity. We observed that the capture gamma ray counts first increased then decreased and varied in different formations; this was especially observed in high-porosity formations. Under the same lithologic conditions (rock matrix), as the porosity increases, the peak value of gamma ray counts moves toward the neutron source. At different detector-source distances, the ratio of the capture gamma ray counts was well correlated with the formation density. An equation of the formation density conversion was established based on the ratio of capture gamma ray counts at the detector-source distances of 30 cm and 65 cm, and the calculated values were consistent with the true values. After correction, the formation density was highly consistent with the true value of the limestone density, and the mean absolute error was 0.013 g/cm³. The calculated porosity values were very close to the true values, and the mean relative error was 2.33%, highlighting the accuracy of the proposed method. These findings provide a new method for developing D-D neutron source logging tools and their well-log data processing methods.

This work was partly supported by the National Natural Science Foundation of China (Nos. 41704113, 41674129), Key R&D Projects in Shandong Province (No. 2019GSF109047), China Postdoctoral Science Foundation Grant (No. 2019M661912), and Science and Technology Plan Project of Shandong Education of China (Nos. J18KA190 and J18KA128).

✉ Yang Li
mtlyab@sdau.edu.cn

¹ College of Resources, Shandong University of Science and Technology, Tai'an 271019, China

² School of Geosciences, China University of Petroleum, Qingdao 266580, China

³ College of Mechanical and Electronic Engineering, Shandong Agricultural University, Tai'an 271018, China

⁴ Department of Nuclear Science and Engineering, Nanjing University of Aeronautics and Astronautics, Nanjing 211106, China

Keywords Density measurement · D-D neutron source · Lithological correction · Porosity prediction

1 Introduction

Density logging is an effective method for porosity determination and lithology indication. With the development of geophysical prospecting for fossil fuels, density logging theories and methods have become increasingly necessary in recent years [1, 2]. In particular, the promotion of health safety and environmental awareness has necessitated the use of different sources in density logging [3–5]. Some research institutions and scholars both in China and abroad have conducted research on the replacement of chemical sources with D-T neutron [6–8] and X-ray sources [9, 10] in density logging, and progress has been made in the establishment of density measurement and correction methods [11–13]. D-D neutron sources are superior to D-T neutron sources; they have the advantages of a long service life, low cost, and non-radioactivity [14, 15]. However, the neutron yield of D-D neutron sources is relatively low, which restricts their development [16, 17]. In recent years, with the increase in the neutron yield of D-D sources, their application in well logging has attracted more attention [18, 19]. D-D-neutron sources can produce high thermal neutron fluxes by interacting with a formation. They are usually directly used in neutron porosity logging [20–22], but their application in density logging is still in the exploration stage. He et al. analyzed the energy spectra of γ -rays generated by the interaction between a D-D neutron source and a formation and found that the spectra of the captured γ -rays and mixed field γ -rays were well correlated with the formation density [23]. Zhang Li studied the feasibility of the use of D-D neutron sources in density logging and factors affecting the spatial distribution of the induced gamma rays [24, 25]. Some Chinese companies and institutes, such as China Oilfield Services Limited, carried out studies on density logging with a controllable D-D neutron source and pointed out that the spatial distribution of the induced γ -rays had a significant impact on the design of logging tools [26]. In the previous studies, the feasibility of density measurement with a controllable D-D neutron source was verified, but the detailed methods for density calculation and correction were not given.

Based on previous studies, this study proposes a method for measuring formation density with a D-D neutron source and correcting the effects of lithology. The Monte Carlo N Particle Transport Code (MCNP) was used to study the characteristics of the spatial distribution of the captured gamma rays in formations of varying lithology. The code was also used to analyze the relationship between the ratio of gamma ray counts and formation density at different detector-source distances and to establish equations for calculating formation density. Finally, using the limestone

data as a reference, density correction values under varying porosity conditions were determined, which laid a solid foundation for accurate porosity calculations. This study provides a reference for the development of controllable D-D neutron source density logging tools and research on their application.

2 Theoretical background

During D-D source density logging, the pulsed neutron generator (nuclear reaction formula: $d + {}^2\text{H} \rightarrow {}^3\text{H} + n$) generates 2.45 MeV fast neutrons, which react with the nuclides in the formation. The γ -rays generated during these reactions are used as the induced γ -ray source to measure the density of the formation. It has been verified that the induced γ -rays are mainly capture γ -rays. Unlike the point source γ -rays used in traditional density logging, capture γ -rays are not single energy rays, and their spatial positions are not fixed. The photons of these spatially distributed capture γ -rays form the γ -ray source for density logging. Capture γ -rays are attenuated after they are generated. The γ -ray flux measured by the detectors can be calculated as follows [27, 28]:

$$\phi_{\gamma} = \frac{1}{2} \sum_a \int_{-\infty}^{+\infty} \int_0^{+\infty} \phi_t \left(\sqrt{r^2 + z^2} \right) \frac{e^{-[\mu \rho_b \sqrt{r^2 + (1-z)^2}]}}{4\pi [r^2 + (1-z)^2]} r dr dz, \quad (1)$$

where ϕ_t is the neutron flux, μ is the γ -ray mass attenuation coefficient, and ρ_b is the bulk density of the formation.

Equation (1) indicates that the responses of capture γ -rays detected by the detectors are related to the macroscopic capture cross section of the formation, the distribution of thermal neutrons, and formation density. Therefore, the ratio of capture gamma ray counts measured by gamma-ray detectors may vary even in formations with the same density. This is mainly because the capture gamma ray counts are affected by both the macroscopic capture cross section of the formation and the spatial distribution of thermal neutrons. Figure 1 shows the distribution of capture gamma ray fluxes in three formations (sandstone, limestone, and dolomite) with the same density ($\rho = 2.65 \text{ g/cm}^3$). The intensity of the capture gamma ray flux is highlighted in colors (high values in red, and low values in blue).

As shown in Fig. 1, in the three formations with the same density, the gamma rays are spatially distributed in different patterns in the zones around the neutron source. In particular, the capture gamma ray flux varies significantly near the detector that was far from the neutron source, demonstrated by the different distributions and ranges of

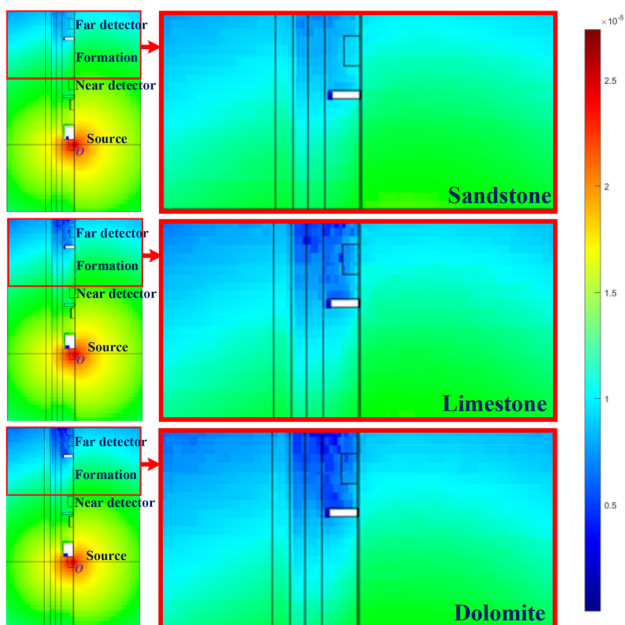


Fig. 1 (Color online) Distributions of capture gamma ray flux in three formations (sandstone, limestone and dolomite) with the same density

colors in the blue area, as shown in the right panels of Fig. 1. The capture gamma ray flux was the lowest in the dolomite formation and the highest in the sandstone formation. When a gamma ray count measured by a single detector is used to determine the formation density, the density measurements have significant errors.

To eliminate the effects of other factors on the density measurement, the ratio of capture γ -ray counts measured by two detectors (near and far detectors) was used to measure the formation density. The relationship between the ratio of capture γ -ray counts measured by the near and far detectors, expressed as R , and the formation density can be obtained using Eq. (1):

$$R = \frac{\phi_{\gamma 1}}{\phi_{\gamma 2}} = \frac{F(\phi_{t1}, \rho_b)}{F(\phi_{t2}, \rho_b)}, \tag{1}$$

where γ_1 and γ_2 are the distances from the near and far detectors to the neutron source, respectively, and ϕ_{t1} and ϕ_{t2} denote the neutron flux measured by the near and far detectors, respectively. R is mainly related to the formation density, but it is also affected by the spatial distribution of neutrons. This study mainly investigates the calculation of the density using the ratio of gamma-ray counts measured by the two detectors.

In nuclear logging, the Monte Carlo method is a commonly used method for studying the reaction process and spatial distribution of particles. MCNP is a general Monte Carlo particle transport code that can be used for the transport of various particles, such as neutrons, photons,

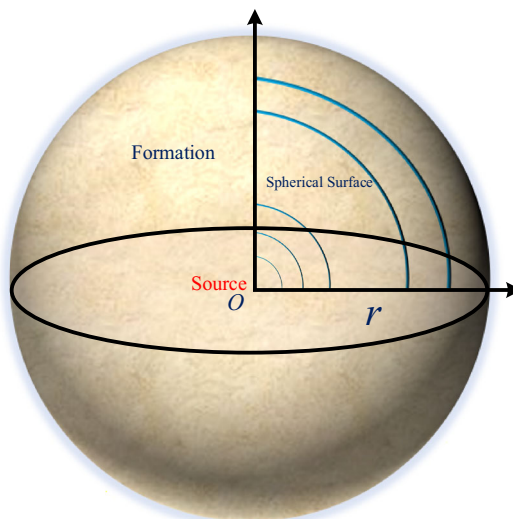


Fig. 2 (Color online) Calculation model

and electrons [29, 30]. In this study, this method was used to study the characteristics of the spatial distribution of capture gamma rays under various formation conditions. We built a pure theoretical model (not considering well-bore and logging instruments) as shown in Fig. 2, which is a sphere and is divided into a number of concentric spheres with a radius difference of 5 cm. The initial radius (detector-source distance) is $r = 5$ cm, and the radius of the outermost sphere is $r = 120$ cm. The neutron source is located at point O , the center of the sphere. Neutrons are directly emitted in the formation. The gamma ray fluxes through the spherical surfaces are recorded. The neutron yield of the D-D neutron generator is 1×10^7 n/s, and the intensity of neutron source is 2.45 MeV.

Three typical formations, namely sandstone, limestone, and dolomite, were used for the simulation. The rock matrices of these formations were SiO_2 , CaCO_3 , and $\text{CaMg}(\text{CO}_3)_2$, respectively. The pore fluid, porosity, and porosity variation steps 2% were H_2O , 0–40%, and 2%. Detailed parameters are listed in Table 1.

The calculation model shown in Fig. 2 was used to record the gamma-ray fluxes through the spherical surfaces under various formation conditions (as listed in Table 1). The gamma-ray counts at different detector-source distances were obtained. The results are shown in Fig. 3.

Figure shows that as the detector-source distance increases, the gamma ray count increases then decreases, but its distribution range is affected by porosity. For pure minerals with a porosity of zero, the capture gamma rays had a wide spatial distribution range. As the porosity increased, the spatial distribution range narrowed, and the peak value of the gamma ray count moved toward the neutron source. When the porosity was 40%, the peak value was closest to the neutron source. The main reason

Table 1 Parameter information of three typical lithologic strata

Sandstone (SiO ₂)		Limestone (CaCO ₃)		Dolomite (CaMg(CO ₃) ₂)	
Pore fluid H ₂ O		Pore fluid H ₂ O		Pore fluid H ₂ O	
Porosity (%)	Density (g/cm ³)	Porosity (%)	Density (g/cm ³)	Porosity (%)	Density (g/cm ³)
0	2.65	0	2.71	0	2.87
2	2.617	2	2.6758	2	2.8326
4	2.584	4	2.6416	4	2.7952
6	2.551	6	2.6074	6	2.7578
8	2.518	8	2.5732	8	2.7204
10	2.485	10	2.539	10	2.683
12	2.452	12	2.5048	12	2.6456
14	2.419	14	2.4706	14	2.6082
16	2.386	16	2.4364	16	2.5708
18	2.353	18	2.4022	18	2.5334
20	2.32	20	2.368	20	2.496
22	2.287	22	2.3338	22	2.4586
24	2.254	24	2.2996	24	2.4212
26	2.221	26	2.2654	26	2.3838
28	2.188	28	2.2312	28	2.3464
30	2.155	30	2.197	30	2.309
32	2.122	32	2.1628	32	2.2716
34	2.089	34	2.1286	34	2.2342
36	2.056	36	2.0944	36	2.1968
38	2.023	38	2.0602	38	2.1594
40	1.99	40	2.026	40	2.122

for this is that water is used as the pore fluid for the numerical simulation. A high porosity indicates a high hydrogen content. The neutrons slowed down quickly. Because there are more thermal neutrons in the zone close to the neutron source, the gamma ray count resulting from thermal neutron capture is high. It should be noted that thermal neutron counts, such as carbon, silicon, and magnesium, are also affected by other elements in the formation. In low-porosity formations, the effects of these elements are not negligible. In pure rock masses, the neutrons slow down over a long time. Hence, when neutrons slow down to become thermal neutrons, they will be far away from the neutron source. Therefore, the peak value of the capture gamma ray count will also be far away from the neutron source. The pattern of the spatial distribution of the capture gamma rays varies in different formations. This is closely related to the elements in the rock matrices of different formations.

3 Relationship between the ratio of capture gamma ray counts and formation density

The gamma ray counts measured in different formations at different detector-source distances were analyzed to obtain the optimal ratio of the gamma ray counts measured by the near and far detectors for calculating the density. As shown in Fig. 3, the peak values of the captured γ -ray counts in different formations were mainly distributed within the range of 20–80 cm. The locations of the peak values represent the main distribution zones of the capture gamma. The relationship between the ratio of the capture gamma ray counts and formation density was analyzed by fitting at different detector-source distances. The results listed in Table 2 show that for formations with the same lithology, the ratio of capture gamma ray counts was highly correlated with the formation density, and the average correlation coefficient was 0.99.

The above analysis shows that in the main gamma capture spatial distribution area between 20 and 80 cm, the gamma count ratio under different source distance combinations had a good correlation with the formation density, especially when the near-source distance was 25–35 cm and the far-source distance was 50–70 cm. In addition, the size of the actual instrument must be also considered,

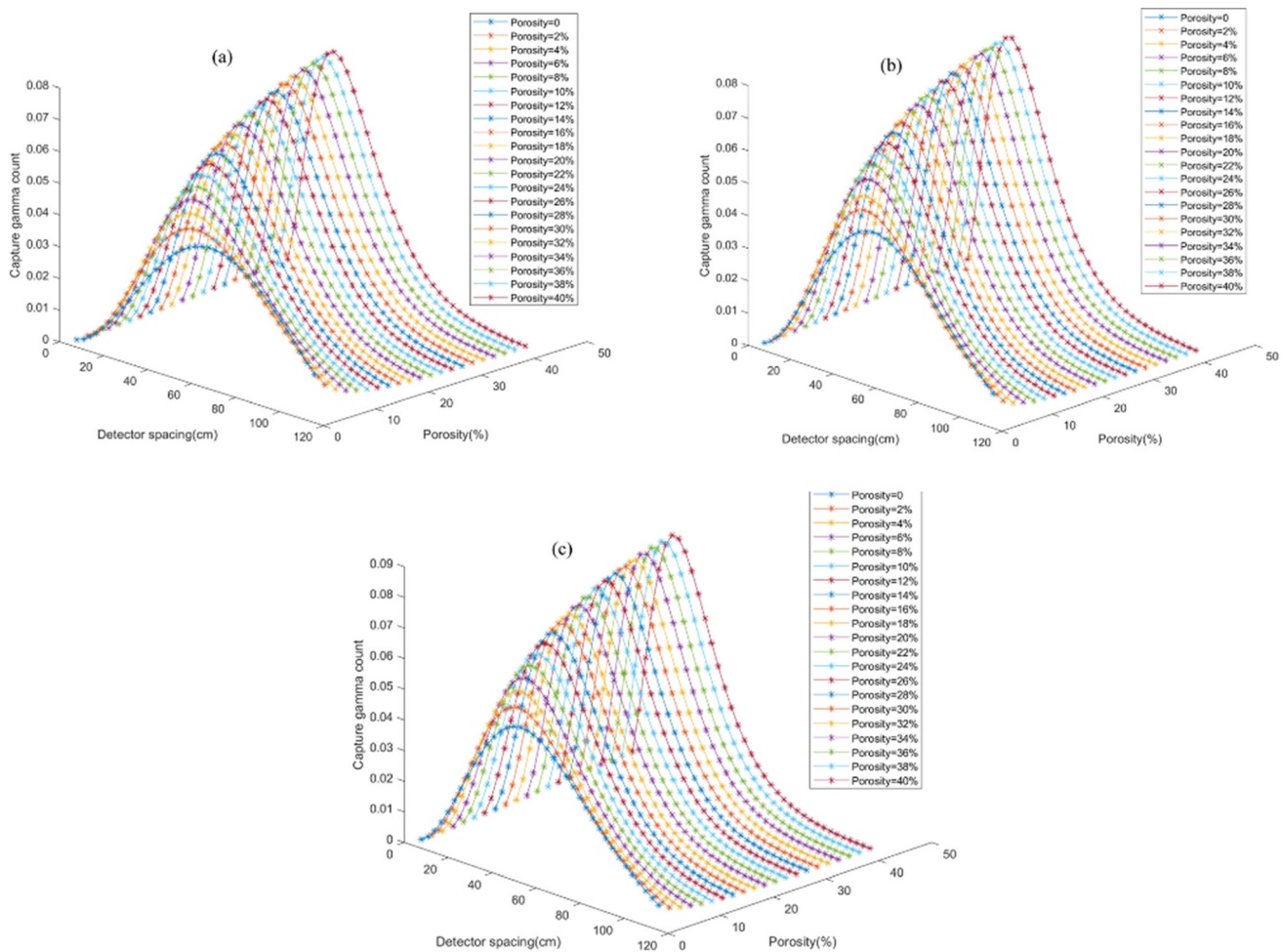


Fig. 3 (Color online) Distribution of capture gamma rays in three different lithologic strata with different source distances: **a.** Sandstone formation, **b.** Limestone formation, **c.** Dolomite formation

including the detector size and thickness of the shield, and the distances of the near and far sources were selected as 30 cm and 65 cm after comparison. Based on the structural design of the logging instrument, a structural model was developed. The model is shown in Fig. 4. The detailed parameters of the model are summarized below. The wellbore had a diameter of 20 cm and was filled with fresh water. The neutron yield of the D-D neutron source was 2×10^7 n/s, and the pulse width was 40 μ s. Two NaI-type gamma-ray detectors were used. The near and far gamma ray detector were 30 and 60 cm away from the D-D neutron source, respectively. The lengths of the near and far detectors were 5 and 10 cm, respectively. Shields were placed between the neutron source and detectors and between the near detector and far detector. These shields were made of tungsten, iron, and nickel materials with a density of 17.78 g/cm³.

Using the model shown in Fig. 4, the ratios of gamma ray counts measured by the near and far detectors in sandstone, limestone, and dolomite formations with

varying porosity (the parameters of these formations are listed in Table 1) were obtained, and the relationship between the ratio of gamma ray counts and formation density was analyzed, as shown in Fig. 5.

The equations for calculating the density of these three formations were found to be

$$\text{Sandstone : } y_d = -0.0016x_c^2 - 0.1197x_c + 2.697, R^2 = 0.9976, \quad (3)$$

$$\text{Limestone } y_d = -0.0075x_c^2 - 0.0637x_c + 2.7371, R^2 = 0.9947, \quad (4)$$

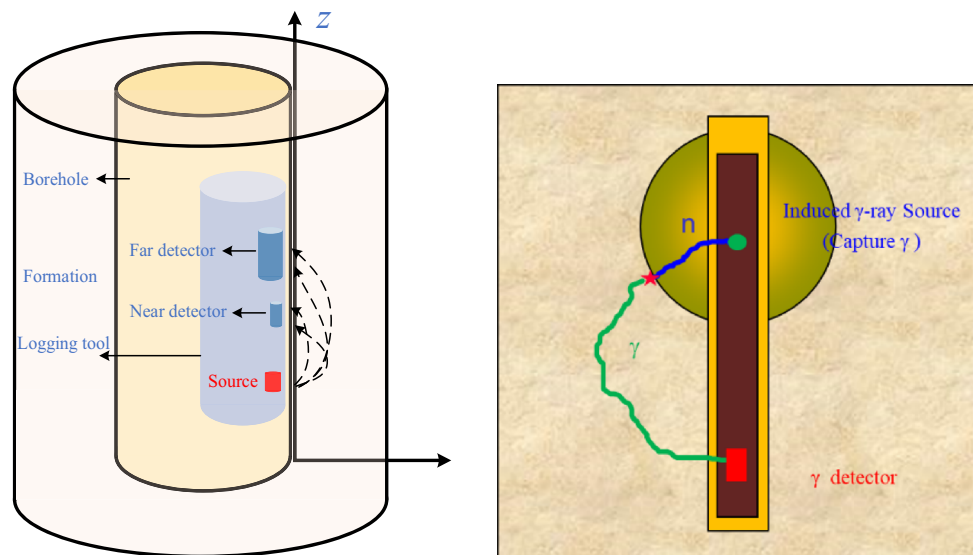
$$\text{Dolomite : } y_d = -0.006x_c^2 - 0.0662x_c + 2.9146, R^2 = 0.9952, \quad (5)$$

where x_c is the capture gamma count ratio between the near and far detectors, and y_d is the formation density.

From Fig. 5 and Eqs. 3–5, it can be seen that in the three formations, the relationship between the ratio of gamma ray counts and formation density follows functions. As the ratio of gamma ray counts increased, the formation density

Table 2 Correlation coefficient of the counting ratio and formation density under 42 different source distance combinations

Various of detector spacing	Sandstone	Limestone	Dolomite	Various of detector spacing	Sandstone	Limestone	Dolomite
20/50	0.9993	0.9989	0.9991	35/65	0.9969	0.9905	0.9927
20/55	0.9990	0.9986	0.9988	35/50	0.9983	0.9949	0.9955
20/60	0.9980	0.9976	0.9979	35/55	0.9983	0.9946	0.9951
20/65	0.9967	0.9963	0.9968	35/60	0.9978	0.9929	0.9938
20/70	0.9959	0.9957	0.9962	35/70	0.9962	0.9893	0.9905
20/75	0.9942	0.9940	0.9945	35/75	0.9949	0.9848	0.9872
20/80	0.9924	0.9922	0.9926	35/80	0.9931	0.9796	0.9823
25/50	0.9994	0.9988	0.9990	40/50	0.9973	0.9923	0.9935
25/55	0.9992	0.9985	0.9987	40/55	0.9974	0.9921	0.9930
25/60	0.9984	0.9975	0.9978	40/60	0.9970	0.990	0.9916
25/65	0.9972	0.9962	0.9966	40/65	0.9960	0.9871	0.9893
25/70	0.9965	0.9955	0.9959	40/70	0.9953	0.9856	0.9876
25/75	0.9950	0.9935	0.9942	40/75	0.9939	0.98	0.9836
25/80	0.9932	0.9914	0.9919	40/80	0.9920	0.9734	0.9775
30/50	0.9992	0.9977	0.9980	45/50	0.9934	0.9832	0.9874
30/55	0.9991	0.9974	0.9976	45/55	0.9943	0.9835	0.9868
30/60	0.9986	0.9962	0.9966	45/60	0.9941	0.9807	0.9850
30/65	0.9976	0.9945	0.9952	45/65	0.9931	0.9766	0.9818
30/70	0.9970	0.9936	0.9943	45/70	0.9923	0.9742	0.9794
30/75	0.9957	0.9908	0.9919	45/75	0.9906	0.9658	0.9737
30/80	0.994	0.9875	0.9887	45/80	0.9883	0.9555	0.9646

Fig. 4 (Color online) Schematic diagram of instrument model

decreased, and the ratio of gamma-ray counts was affected by the formation porosity. Furthermore, the gamma ray counts measured by the near and far detectors were high for greater porosity. This is because the hydrogen content of the formation increases with increasing porosity, which slows neutrons quicker, increasing the thermal neutron flux

close to the near detector and number of gamma rays from thermal neutron capture. On the other hand, the gamma ray count measured by the far detector decreased with greater porosity accordingly. Therefore, the ratio of gamma ray counts measured by the near and far detectors increases. In the three formations, the ratio of gamma ray counts has a

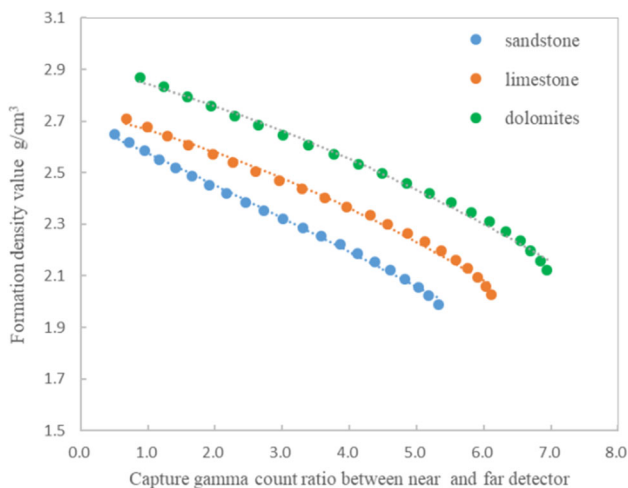


Fig. 5 (Color online) Relationship between the capture gamma ray count ratio and formation density for the source distance combination of 30/65 cm

good fit with the formation density, but the effects of lithology are significant. To obtain accurate information on the formation density through density logging, the effects of lithology must be corrected.

4 Method for correcting the effects of lithology

Formation density data are frequently used in geophysical prospecting to obtain porosity. However, it is very difficult to precisely transform the density data to the porosity because the density is strongly affected by mineral composition. The inaccuracies of matrix density will have a significant impact on the calculated porosity. To determine the porosity of formations accurately, it is usually necessary to convert the density logs to values relative to a certain standard lithology in order to eliminate the impact of inappropriately selected matrix parameters on the calculation results.

First, the densities of sandstone, limestone, and dolomite formations with varying porosities were calculated using the equations for calculating the formation density. Second, the values for correcting the effects of lithology on the densities of the three formations for varying porosities were calculated. The results are shown in Table 3.

From Table 3, it can be seen that for formations with varying porosity, different values should be used to correct the effects of lithology on density. The calculated density of the sandstone formation was slightly higher than the true value, and that of the dolomite formation was slightly lower than the true value. Therefore, the value for correcting the effects of lithology in the sandstone formation is negative, and that for correcting the effects of lithology in the dolomite formation is positive. The relationship

between the porosity values of these three formations and the corresponding correction values was analyzed, as shown in Fig. 6. The fit equations are as follows:

$$\begin{aligned}
 \text{Sandstone : } \Delta y_d &= -6.8665x_p^3 + 4.0612x_p^2 - 0.6846x_p \\
 &+ 0.0782, R^2 \\
 &= 0.9733,
 \end{aligned} \tag{6}$$

$$\begin{aligned}
 \text{Limestone : } \Delta y_d &= -10.431x_p^3 + 5.9817x_p^2 - 0.8797x_p \\
 &+ 0.0235 R^2 \\
 &= 0.9802,
 \end{aligned} \tag{7}$$

$$\begin{aligned}
 \text{Dolomite : } \Delta y_d &= -10.838x_p^3 + 6.2223x_p^2 - 0.7575x_p \\
 &- 0.1354, R^2 \\
 &= 0.9859,
 \end{aligned} \tag{8}$$

where x_p is the porosity, and Δy_d is the density correction value.

From Fig. 6, it can be seen that for the three formations, the value of the density correction is well correlated with the porosity. The density correction value of the limestone formation was the smallest, which is a result of statistical errors. The density correction value of the dolomite formation was large. When the porosity was lower than 40%, this value was equal to or smaller than 0.16 g/cm³. The density correction value of the sandstone formation was moderate. As the porosity increased, this value decreased, and when the porosity was 40%, it was 0.0122 g/cm³. Using the density correction values of the three formations, the formation porosity can be accurately calculated to quantitatively determine the formation parameters.

To validate the accuracy of the density measurements and corrections of the lithology effect on porosity, the densities and porosities of sandstone, limestone, and dolomite formations (the pore fluid is water) with porosities of 3%, 5%, 13%, 15%, 23%, 25%, 33%, and 35% were calculated using the Monte Carlo numerical simulation and the model shown in Fig. 4. The calculated values were compared with theoretical values. The results are shown in Figs. 7 and 8, respectively.

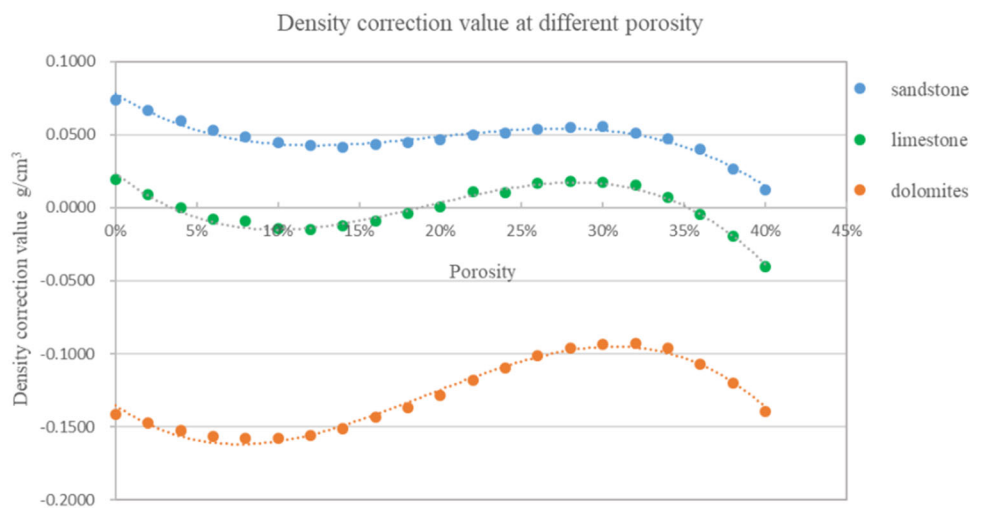
Figure 7 shows that almost all the density values calculated with the density calculation equations fall on the 45° line, and these calculated values are highly consistent with the true values, which verifies the accuracy of the equations. Lithology has a significant impact on the calculated density values, and the density measurement errors affect the porosity calculation.

Figure 8 shows the comparison of the porosity values of the sandstone and dolomite formations calculated before and after the effects of lithology were corrected. In Fig. 8, the porosity values of the sandstone and dolomite

Table 3 Three lithologic and stratigraphic density corrections

Porosity (%)	Sandstone			Limestone			Dolomite		
	True density (g/cm ³)	Calculated density (g/cm ³)	Deviation	True density (g/cm ³)	Calculated density (g/cm ³)	Deviation	True density (g/cm ³)	Calculated density (g/cm ³)	Deviation
0	2.65	2.70	-0.05	2.71	2.69	0.02	2.87	2.69	0.18
2	2.62	2.69	-0.07	2.68	2.67	0.01	2.83	2.65	0.18
4	2.58	2.67	-0.09	2.64	2.64	0.00	2.80	2.62	0.18
6	2.55	2.65	-0.10	2.61	2.62	-0.01	2.76	2.59	0.17
8	2.52	2.64	-0.12	2.57	2.58	-0.01	2.72	2.55	0.17
10	2.49	2.62	-0.14	2.53	2.56	-0.03	2.68	2.51	0.17
12	2.45	2.59	-0.14	2.50	2.52	-0.01	2.65	2.47	0.17
14	2.42	2.57	-0.15	2.47	2.48	-0.01	2.61	2.43	0.18
16	2.39	2.54	-0.15	2.44	2.44	0.00	2.57	2.38	0.19
18	2.35	2.51	-0.16	2.40	2.40	0.00	2.53	2.33	0.20
20	2.32	2.49	-0.17	2.37	2.37	-0.01	2.50	2.28	0.21
22	2.29	2.45	-0.16	2.33	2.31	0.02	2.46	2.23	0.23
24	2.25	2.41	-0.16	2.30	2.28	0.02	2.42	2.19	0.24
26	2.22	2.38	-0.16	2.27	2.24	0.03	2.38	2.14	0.25
28	2.19	2.35	-0.16	2.23	2.20	0.03	2.35	2.09	0.25
30	2.16	2.32	-0.17	2.20	2.19	0.01	2.31	2.05	0.25
32	2.12	2.28	-0.16	2.16	2.14	0.02	2.27	2.02	0.25
34	2.09	2.26	-0.17	2.13	2.12	0.01	2.23	1.99	0.25
36	2.06	2.23	-0.17	2.09	2.10	0.00	2.20	1.97	0.23
38	2.02	2.21	-0.19	2.06	2.09	-0.03	2.16	1.95	0.21
40	1.99	2.20	-0.21	2.03	2.09	-0.06	2.12	1.93	0.19

Fig. 6 (Color online) Density corrections for sandstone, limestone, and dolomite for different porosity



formations calculated before correction are distributed on both sides of the 45° line, and the data points of the dolomite formation are farther from this line. After corrections are made, the calculated values of porosity are

highly consistent with the true values and most fall on the 45° line. Figure 9 shows the relative errors of the calculated porosity values of the sandstone and dolomite formations. In Fig. 9, when porosity is less than 5%, the

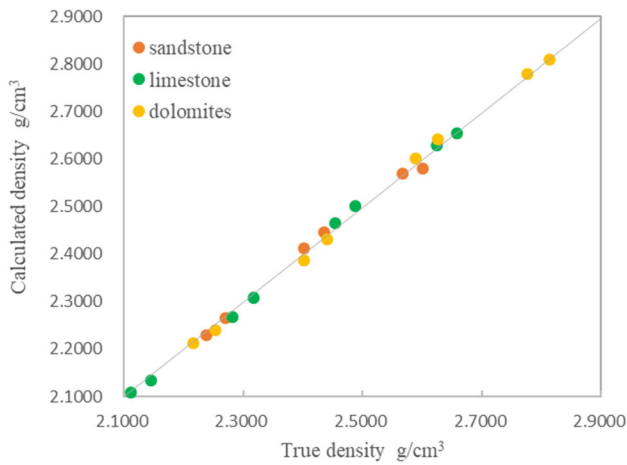


Fig. 7 (Color online) The relationship between the calculated and true density values is obtained using the density fitting formula

relative errors are significant but smaller than 5%. Only the relative error of the calculated porosity of sandstone reaches 30%, which is related to the cumulative error in the density measurement. When porosity is higher than 5%, the relative errors in the calculated porosity values smaller than 4%, indicating that the correction method is effective. The formation porosity parameters obtained during density measurements with a D-D neutron source indicate that the effects of lithology are not negligible, and they are greater in low-porosity formations. Therefore, the effects of lithology must be corrected to obtain accurate formation parameters.

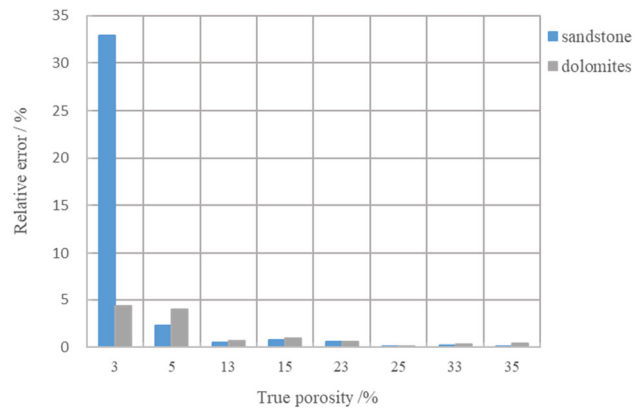


Fig. 9 (Color online) Relative error of the calculated porosity before and after correction

5 Conclusion

In density measurements with a D-D neutron source, lithology has a significant impact on the spatial distribution of capture gamma rays. In formations with the same lithology, the spatial distribution of capture gamma rays follows certain rules. In formations with varying lithologies, the spatial distribution of capture gamma rays varies significantly. Through an analysis using a neutron source-formation model, it was found that when porosity is within the range of 0–40%, the capture gamma rays in the three typical formations are mainly distributed within the range of 20–80 cm away from the neutron source.

The ratio of gamma ray counts measured by two gamma-ray detectors can be used to determine the formation density. The ratio of capture gamma ray counts was highly correlated with the formation density, and the correlation coefficient was 0.99. However, the density measurement was affected by the lithology. For formations with varying lithologies, different equations were used to calculate the density.

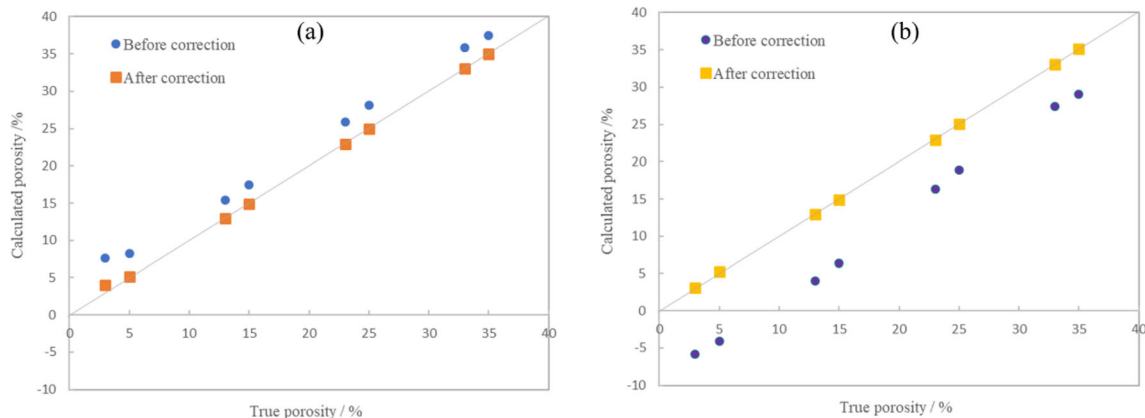


Fig. 8 (Color online) Comparison of the calculated and true porosity values before and after correction: (a) Sandstone, (b) Dolomite

The accuracy of the equations for calculating the formation density and correcting the effects of lithology on porosity was verified using the simulation data. The mean error of the density values obtained from the density calculation equations was smaller than 0.015 g/cm^3 , which satisfies the density measurement requirements. After the effects of lithology were corrected, the mean relative errors of the calculated formation porosity were smaller than 4%. This shows that the proposed correction method can effectively reduce the effects of lithology on the porosity calculation and improve the accuracy of the formation parameters.

Author contributions All authors contributed to the study conception and design. Material preparation, data collection and analysis were performed by Li Zhang, Hua-Wei Yu, Yang Li, Wen-Bao Jia, Xiao Han, Xue-Sen Geng. The first draft of the manuscript was written by Li Zhang and all authors commented on previous versions of the manuscript. All authors read and approved the final manuscript.

References

1. M. Evans, R. Adolph, L. Vildé et al., A sourceless alternative to conventional LWD nuclear logging. SPE Annual Technical Conference and Exhibition, Dallas, Texas, October 2000, SPE 62982-MS (2000). <https://doi.org/10.2118/62982-MS>
2. H. Peng, Review on progress of radioactive well logging technology in 2000–2008. Well Logg. Technol. **33**(1), 1–8 (2009). <https://doi.org/10.16489/j.issn.1004-1338.2009.01.00> (in Chinese)
3. J.D. Aitken, R. Adolph, M. Evans et al., Radiation sources in drilling tools: comprehensive risk analysis in the design, development and operation of LWD tools. SPE International Conference on Health, Safety and Environment in Oil and Gas Exploration and Production, March 20–22 (2002). <https://doi.org/10.2118/73896-MS>
4. A. Badruzzaman, S. Bames, F. Bair et al., Radioactive sources in petroleum industry: applications, Concerns and Alternatives. Asia Pacific Health, Safety, Security and Environment Conference, 4–6 (2009). <https://doi.org/10.2118/123593-MS>
5. Non-isotopic alternative technologies working group. Non-Radio isotopic alternative technologies white paper. U.S. Department of Homeland Security Cybersecurity and Infrastructure Security Agency (2019)
6. R.D. Wilson, Bulk density logging with high-energy gammas produced by fast neutron reactions with formation oxygen atoms. In: Proceeding of Nuclear Science Symposium and Medical Imaging Conference, (San Francisco), 209–213 (1995). <https://doi.org/10.1109/NSSMIC.1995.504211>
7. R.C. Odom, D.E. Tiller, R.D. Wilson, Improvements in a through-casing pulsed-neutron density log. SPE Annual Technical Conference and Exhibition, New Orleans, Louisiana, September 2001, SPE-71742-MS (2001). <https://doi.org/10.2118/71742-MS>
8. H.W. Yu, J.M. Sun, J.X. Wang et al., Accuracy and borehole influences in pulsed neutron gamma density logging while drilling. Appl. Radiat. Isot. **69**, 1313–1317 (2011). <https://doi.org/10.1016/j.apradiso.2011.04.023>
9. F. Zhang, Y.F. Li, Y. Xin et al., Numerical simulation of density logging based on X-ray and gamma ray sources. J. China Univ. Pet. **42**(01), 60–66 (2018). <https://doi.org/10.3969/j.issn.1673-5005.2018.01.007>
10. H.W. Yu, X.H. Chen, Y. Zhou et al., Impact of photoelectric effect on X-ray density logging and its correction. Appl. Radiat. Isot. **156**, 108785 (2020). <https://doi.org/10.1016/j.apradiso.2019.06.031>
11. B.Z. Pan, R. Zhang, K. Liu et al., Numerical simulation of pulsed neutron source density logging's secondary capture gamma ray strength. Geophys. Prospect. Pet. **53**(6), 642–648 (2014). <https://doi.org/10.3969/j.issn.1000-1441.2014.06.003> (in Chinese)
12. F. Zhang, Q.Y. Zhang, J.T. Liu et al., A method to describe inelastic gamma field distribution in neutron gamma density logging. Appl. Radiat. Isot. **129**, 189–195 (2017). <https://doi.org/10.1016/j.apradiso.2017.08.024>
13. H.W. Yu, Y.X. Zhang, X.H. Chen et al., Numerical simulation and method study of X-ray litho-density logging. Nucl. Sci. Tech. **31**(12), 124 (2020). <https://doi.org/10.1007/s41365-020-00826-2>
14. Z.-W. Huang, J.-R. Wang, Z. Wei et al., Development of a compact D-D neutron generator. J. Instrum. **13**(1), P01013 (2018). <https://doi.org/10.1088/1748-0221/13/01/P01013>
15. Y. Gong, X.C. Guan, Q. Wang et al., Design of moderator for boron neutron capture therapy based on D-D neutron source. Nucl. Tech. **43**(9), 090303 (2020). <https://doi.org/10.11889/j.0253-3219> (in Chinese)
16. L. Bond, K. Denslow, J. Griffin et al., *Evaluation of non-nuclear techniques for well logging technology evaluation* (PNNL, Washington, 2010). <https://doi.org/10.2172/1006309>
17. J. Griffin, T. Moran, L. Bond, *Radiation source replacement workshop* (PNNL, Washington, 2010). <https://doi.org/10.2172/1062523>
18. C.R. Peeples, M. Mickael, R.P. Gardner, On replacing Am-Be neutron sources in compensated porosity logging tools. Appl. Radiat. Isot. **68**(4–5), 926–931 (2010). <https://doi.org/10.1016/j.apradiso.2009.11.042>
19. A.X. Chen, A.J. Antolak, K.-N. Leung, Electronic neutron sources for compensated porosity well logging. Nucl. Instrum. Meth. A **684**, 52–56 (2012). <https://doi.org/10.1016/j.nima.2012.04.053>
20. F. Zhang, C. Yuan, Monte Carlo simulation on compensated neutron porosity logging with D-D neutron porosity logging with D-D neutron generator. Well Logg. Technol. **34**(3), 227–232 (2010). <https://doi.org/10.16489/j.issn.1004-1338.2010.03.004> (in Chinese)
21. Y. Yan, B.Y. Li, S.P. Zheng et al., Monte Carlo simulation of the neutron porosity logging using D-D neutron generator. J. Lanzhou Univ. (Nat. Sci.) **48**(03), 123–127 (2012). <https://doi.org/10.13885/j.issn.0455-2059.2012.03.009> (in Chinese)
22. A. Badruzzaman, A. Schmidt, A. Antolak et al., Neutron generator as alternatives to Am-Be source in well logging: an assessment of fundamentals. Petrophysics **60**(1), 136–170 (2019). <https://doi.org/10.30632/PJV60N1-2019a10>
23. X.Y. He, D.P. Xu, Q. Xie et al., Monte Carlo simulation of n- γ density logging of D-D neutron generator. Nucl. Phys. Rev. **30**(02), 151–155 (2013). <https://doi.org/10.11804/NuclPhysRev.30.02.151> (in Chinese)
24. L. Zhang, H.W. Yu, Effect of density measurement on D-D induced gamma counting. Nucl. Tech. **39**(3), 030502 (2016). <https://doi.org/10.11889/j.0253-3219.2016.hjs.39.030502> (in Chinese)
25. L. Zhang, H.W. Yu, W.B. Jia et al., Study on the influence of formation factors on spatial distribution of D-D induced γ -ray source. Nucl. Tech. **42**(1), 010501 (2019). <https://doi.org/10.11889/j.0253-3219> (in Chinese)
26. L. Zhang, H.W. Yu, W.B. Jia et al., A research on the effects of formation elements on the spatial distribution of D-D induced γ -ray source. Appl. Radiat. Isot. **151**, 289–298 (2019). <https://doi.org/10.1016/j.apradiso.2019.06.007>

27. X.G. Han, R. Pemper, T. Tutt et al., Environmental corrections and system calibration for a new pulsed-neutron mineralogy instrument. SPWLA 50th Annual Logging Symposium, 21–24, (2009)
28. F. Zhang, *Foundations of nuclear geophysics* (Petroleum industry press, Beijing, 2015). (in Chinese)
29. R.P. Gardner, L. Xu, Status of the Monte Carlo library least-squares (MCLS) approach for non-linear radiation analyzer problems. *Radiat. Phys. Chem.* **78**(10), 843–851 (2009). <https://doi.org/10.1016/j.radphyschem.2009.04.023>
30. T.B. Yang, M. Wang, X.Y. Fan et al., MCNP simulation for gamma-ray buildup factors of shielding material. *Nucl. Tech.* **44**(3), 030503 (2021). <https://doi.org/10.11889/j.0253-3219> (in Chinese)